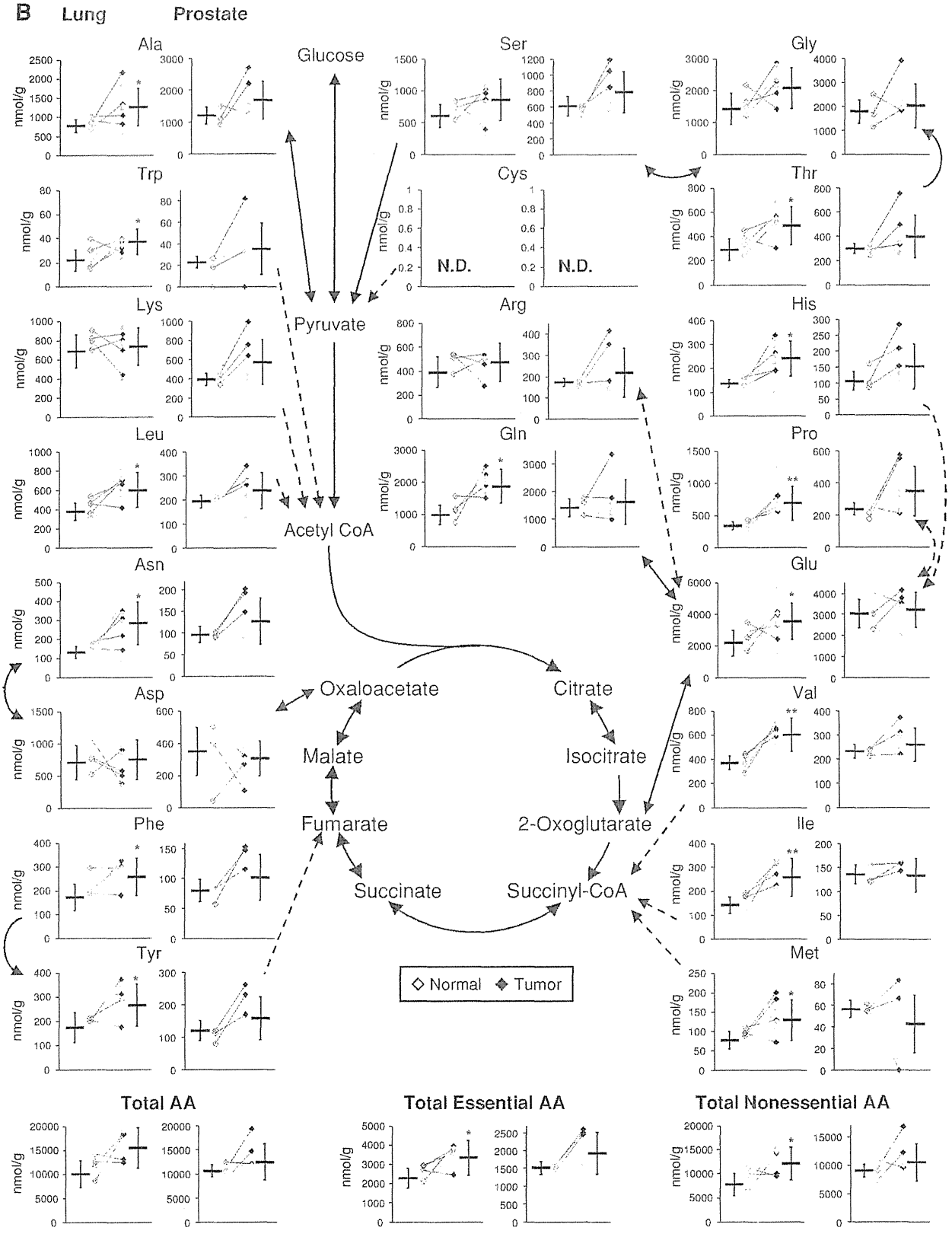

Fig. 1 continued

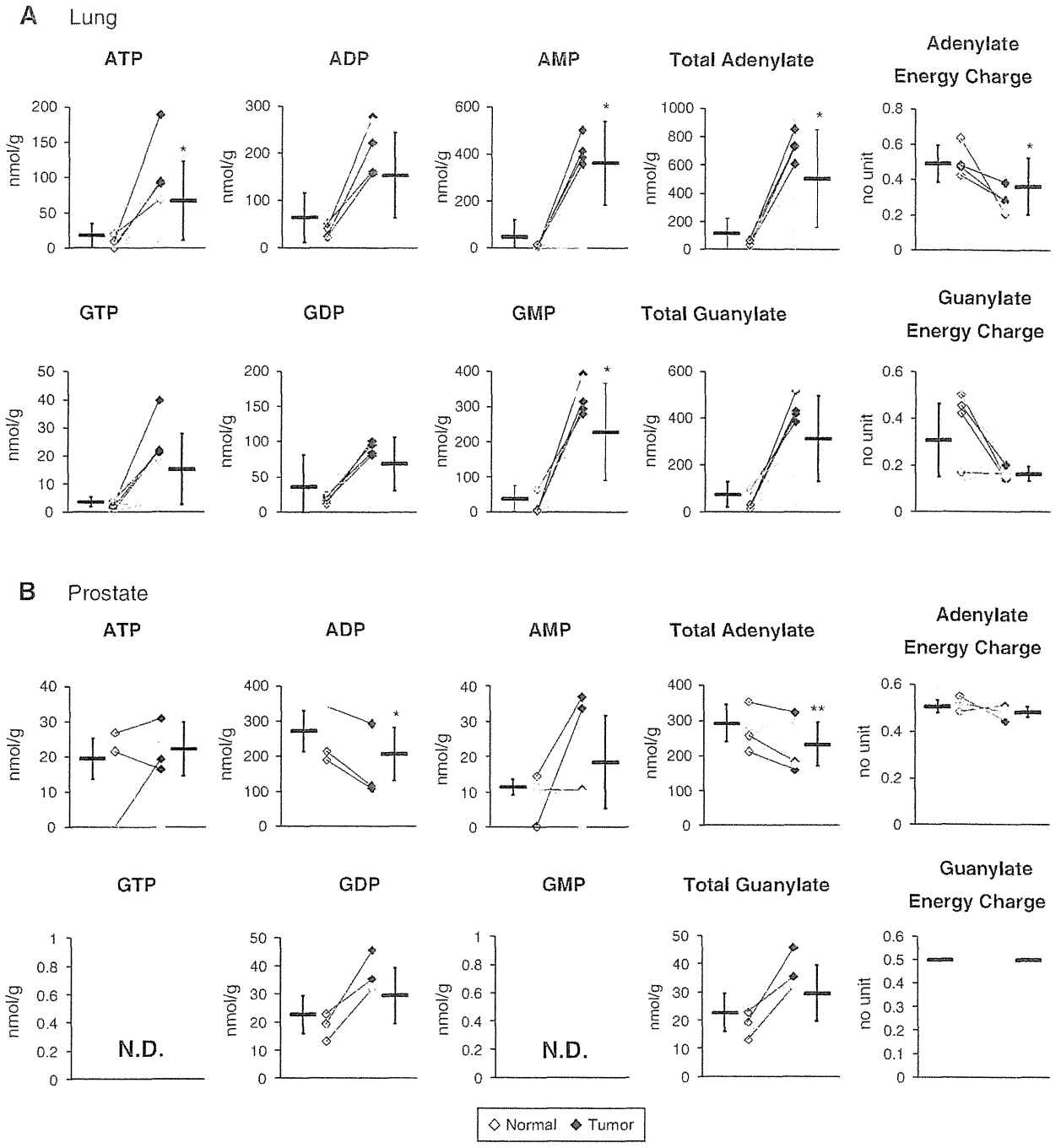

Fig. 2 Adenosine and guanosine phosphates, total adenylates and guanylates, and adenylate and guanylate energy charges of normal (*left, open dots*) and tumor (*right, filled dots*) tissues obtained from lung (**a**) and prostate (**b**) cancer patients. *Horizontal bars* represent mean ± SD of normal (*left*) and tumor (*right*) samples and each connected pair represents the values for the same patient. *Gray dots* represent the values for patients with non-SCC lung cancer (L4–L6, L8 and L9) and patients with moderately differentiated prostate cancer (P1 and P5–7). *N.D.* indicates that the metabolite level was below the detection limit of the analysis. *Asterisks* indicate the significant differences between normal and tumor tissue levels based on the Wilcoxon signed-rank test (*$p < 0.05$; **$p < 0.01$; and ***$p < 0.001$)

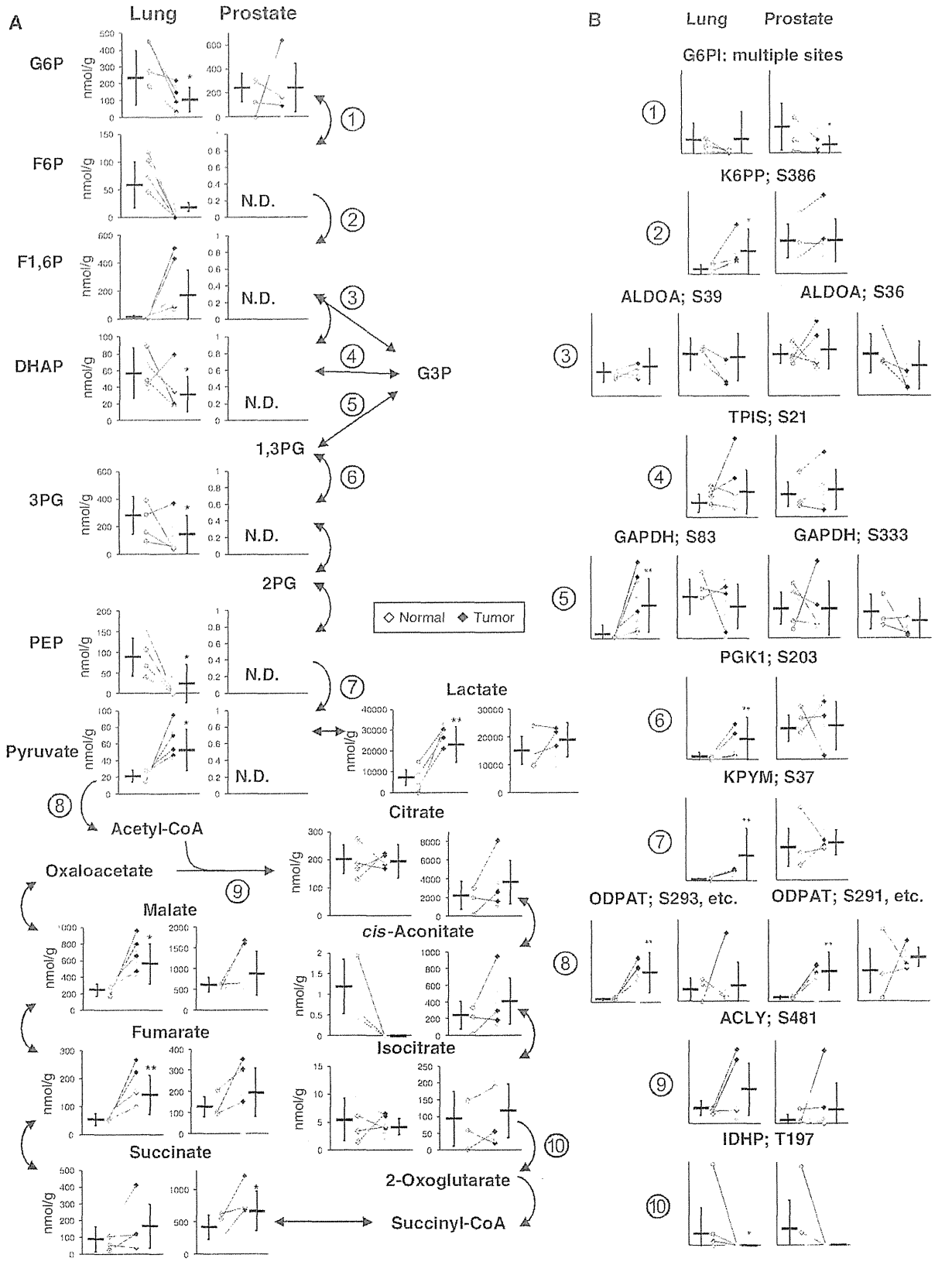
A
Lung
Prostate
G6P
F6P
F1,6P
DHAP
G3P
1,3PG
3PG
2PG
PEP
Pyruvate
Lactate
Citrate
Acetyl-CoA
Oxaloacetate
Malate
cis-Aconitate
Fumarate
Isocitrate
Succinate
2-Oxoglutarate
Succinyl-CoA
N.D.
nmol/g
◇ Normal ◆ Tumor
B
Lung
Prostate
G6PI: multiple sites
K6PP; S386
ALDOA; S39
ALDOA; S36
TPIS; S21
GAPDH; S83
GAPDH; S333
PGK1; S203
KPYM; S37
ODPAT; S293, etc.
ODPAT; S291, etc.
ACLY; S481
IDHP; T197

◀ **Fig. 3** Quantified levels of glycolytic and TCA cycle intermediates (**a**) and phosphorylation levels of each phosphorylation site in associated enzymes (**b**) in normal (*left, open dots*) and tumor (*right, filled dots*) tissues obtained from lung and prostate cancer patients. *Encircled numbers* in (**a**) indicated next to the metabolic reactions involved in glycolysis and the TCA cycle correspond to the associated enzymes in (**b**). *Horizontal bars* represent mean ± SD of normal (*left*) and tumor (*right*) samples and each connected pair represents the values for the same patient. *Gray dots* represent the values for patients with non-SCC lung cancer (L4–L6, L8 and L9) and patients with moderately differentiated prostate cancer (P1 and P5–7). *N.D.* indicates that the metabolite level was below the detection limit of the analysis. *Asterisks* indicate the significant differences between normal and tumor tissue levels based on the Wilcoxon signed-rank test (*$p < 0.05$; **$p < 0.01$; and ***$p < 0.001$). *G6PI* glucose 6-phosphate isomerase; *K6PP* 6-phosphofructokinase; *ALDOA* aldolase A; *TPIS* triosephosphate isomerase; *GAPDH* glyceraldehydes 3-phosphate dehydrogenase; *PGK1* phosphoglycerate kinase 1; *KPYM* pyruvate kinase isozymes M1/M2; *ODPAT* pyruvate dehydrogenase E1 component subunit alpha; *ACLY* ATP-citrate synthase; and *IDHP* isocitrate dehydrogenase

and L7, and their citrate concentrations. The impact of elevated phosphorylation levels of T197 in isocitrate dehydrogenase in normal L2 and P2 samples was also unclear. We need a larger number of sample sets in order to validate these results and provide further insight into possible correlations between phosphorylated states of the enzymes and metabolomic profiles.

Levels of all the quantified TCA cycle intermediates were higher in tumor than normal prostate tissues (Fig. 3a), which may be related to the typically hypoxic microenvironment of prostate tissues, because most TCA cycle intermediates are known to increase under hypoxia, while their flux through the pathway remains low (Wiebe et al. 2008). Average prostate citrate concentrations were >11-fold higher than in lung. This was partly due to a high concentration of zinc in the prostate, which inhibits m-aconitase and results in citrate accumulation (Mycielska et al. 2009). Prostate tumor exhibits low zinc levels and elevated fatty acid synthesis consuming citrate, and thus its citrate level is typically lower than in normal tissues (Mycielska et al. 2009), which is, however, inconsistent with our results. Tumor citrate, *cis*-aconitate, and isocitrate levels in P1, P3 and P7 were consistently lower than their respective normal levels, leaving the possibility that zinc and m-aconitase activity levels may vary depending on a factor other than differentiation status.

Succinate, fumarate, and malate levels were markedly higher in both prostate and lung tumor tissues than their corresponding normal tissues (Fig. 3a), which was consistent with our previous results for colon and stomach tumor metabolomics (Hirayama et al. 2009). We recently obtained strong evidence that, especially under hypoxic and nutrient-deprived conditions, energy generation of cancer relies on fumarate respiration (Sakai et al. 2012; Tomitsuka et al. 2010). This confers upon cells the ability to produce ATP by harnessing fumarate to succinate conversion, rather than oxygen to water, as the final electron transport step via the reverse reaction of succinate dehydrogenase (Kita and Takamiya 2002). Accumulation of these metabolites in tumors may therefore be attributed to hyperactivity of fumarate respiration.

3.4 Tumor-specificity and organ-dependency in metabolic profiles

The metabolome data obtained from both lung and prostate tissues were collectively normalized and hierarchically clustered (Supplementary Fig. S4A). As a result, lung-versus-prostate differences in terms of the overall metabolomic profiles appeared to be more significant than normal-versus-tumor differences within the same organ, as observed in our previous comparative metabolome analyses in colon and stomach tissues (Hirayama et al. 2009). As expected, PCA with the collectively normalized data showed clear inter-organ differences along with the PC2 axis; however, the normal-versus-tumor distinctions were also observed along with the PC1 axis (Supplementary Fig. S4B). This suggests that, in the carcinogenic process, cells alter their metabolism with a certain 'metabolic directionality' that is independent of organ types while retaining much of the metabolism that is unique to their organs of origin. Metabolites that showed high correlations with the PC2 included several nucleosides, TCA cycle intermediates, and polyamines, which characterize the inter-organ metabolic differences (Supplementary Table S3). In contrast, most glucogenic amino acids such as Thr, Ile, Asn, Pro, His, Gln, and Ser were closely associated with the PC1 (Supplementary Table S3), suggesting that a hyper-production and/or -acquisition of a certain set of amino acids likely occurs in the course of tumorigenesis.

4 Conclusion

Overall tumor metabolomic profiles were found to be significantly different depending on tumor type in lung cancer and differentiation status in prostate cancer. Elevated tumor concentrations of almost all the amino acids, especially BCAAs, were identified in an organ-independent manner, and this trend was more prominent in SCC than the other tumor types in lung cancer and in poorly rather than moderately differentiated prostate cancer. Analyses with much more samples, however, are necessary in order to statistically confirm these unique subtype-specific metabolic fingerprint of cancer. In contrast, through our combined metabolomic and phosphorylated enzyme analyses, we found that glycolytic and TCA cycle intermediates,

levels of which are probably associated with enzyme phosphorylation levels, exhibited significant organ dependency, reaffirming that inter-organ metabolomic differences are generally more significant than normal-versus-tumor differences within the same organ. Nonetheless, metabolomic profiles of both lung and prostate tumors appear to have a common 'directionality' along with their increasing malignancy represented by high concentrations of a certain set of glucogenic amino acids. Taken together, we identified organ-dependent, tumor-specific, and tumor-pathology-dependent metabolic features, which highlights the need for a combined metabolomics and phosphoproteomics analysis on a broader scale with a larger number of sample sets for improving specificity and effectiveness of personalized anticancer therapeutics.

Acknowledgments The authors thank Dr. Masahiro Sugimoto for developing MasterHands software. This work was supported in part by a grant for the Third Term Comprehensive 10-year Strategy for Cancer Control from the Ministry of Health, Labour and Welfare (H.E.) and a grant from the Global COE Program entitled, "Human Metabolomic Systems Biology" (K.K.). This work was also supported by KAKENHI (Grant-in-Aid for Scientific Research) on Priority Areas "Systems Genomes" and on "Lifesurveyor" from the Ministry of Education, Culture, Sports, Science and Technology (MEXT) of Japan as well as research funds from the Yamagata prefectural government and the City of Tsuruoka (Y.O., M.T., and T.S.).

References

Baracos, V. E., & Mackenzie, M. L. (2006). Investigations of branched-chain amino acids and their metabolites in animal models of cancer. *Journal of Nutrition, 136*, 237S–242S.

Brand, I. A., & Soling, H. D. (1975). Activation and inactivation of rat liver phosphofructokinase by phosphorylation—dephosphorylation. *FEBS Letters, 57*, 163–168.

Fuchs, B. C., & Bode, B. P. (2005). Amino acid transporters ASCT2 and LAT1 in cancer: Partners in crime? *Seminars in Cancer Biology, 15*, 254–266.

Hall, M., Mickey, D. D., Wenger, A. S., & Silverman, L. M. (1985). Adenylate kinase: An oncodevelopmental marker in an animal model for human prostatic cancer. *Clinical Chemistry, 31*, 1689–1691.

Heiden, M. G. V., Cantley, L. C., & Thompson, C. B. (2009). Understanding the Warburg effect: The metabolic requirements of cell proliferation. *Science, 324*, 1029–1033.

Hirayama, A., Kami, K., Sugimoto, M., Sugawara, M., Toki, N., Onozuka, H., et al. (2009). Quantitative metabolome profiling of colon and stomach cancer microenvironment by capillary electrophoresis time-of-flight mass spectrometry. *Cancer Research, 69*, 4918–4925.

Ishihama, Y. (2005). Proteomic LC-MS systems using nanoscale liquid chromatography with tandem mass spectrometry. *Journal of Chromatography A, 1067*, 73–83.

Ishihama, Y., Rappsilber, J., Andersen, J. S., & Mann, M. (2002). Microcolumns with self-assembled particle frits for proteomics. *Journal of Chromatography A, 979*, 233–239.

Junker, B. H., Klukas, C., & Schreiber, F. (2006). VANTED: A system for advanced data analysis and visualization in the context of biological networks. *BMC Bioinformatics, 7*, 109.

Kita, K., & Takamiya, S. (2002). Electron-transfer complexes in *Ascaris* mitochondria. *Advances in Parasitology, 51*, 95–131.

Korotchkina, L. G., & Patel, M. S. (2001). Site specificity of four pyruvate dehydrogenase kinase isoenzymes toward the three phosphorylation sites of human pyruvate dehydrogenase. *Journal of Biological Chemistry, 276*, 37223–37229.

Kyono, Y., Sugiyama, N., Imami, K., Tomita, M., & Ishihama, Y. (2008). Successive and selective release of phosphorylated peptides captured by hydroxy acid-modified metal oxide chromatography. *Journal of Proteome Research, 7*, 4585–4593.

Le Mellay, V., Houben, R., Troppmair, J., Hagemann, C., Mazurek, S., Frey, U., et al. (2002). Regulation of glycolysis by Raf protein serine/threonine kinases. *Advances in Enzyme Regulation, 42*, 317–332.

Mycielska, M. E., Patel, A., Rizaner, N., Mazurek, M. P., Keun, H., Ganapathy, V., et al. (2009). Citrate transport and metabolism in mammalian cells: Prostate epithelial cells and prostate cancer. *BioEssays, 31*, 10–20.

Ohashi, Y., Hirayama, A., Ishikawa, T., Nakamura, S., Shimizu, K., Ueno, Y., et al. (2008). Depiction of metabolome changes in histidine-starved *Escherichia coli* by CE-TOFMS. *Molecular BioSystems, 4*, 135–147.

Olsen, J. V., de Godoy, L. M., Li, G., Macek, B., Mortensen, P., Pesch, R., et al. (2005). Parts per million mass accuracy on an Orbitrap mass spectrometer via lock mass injection into a C-trap. *Molecular and Cellular Proteomics, 4*, 2010–2021.

Patel, M. S., & Korotchkina, L. G. (2001). Regulation of mammalian pyruvate dehydrogenase complex by phosphorylation: Complexity of multiple phosphorylation sites and kinases. *Experimental & Molecular Medicine, 33*, 191–197.

Rappsilber, J., Ishihama, Y., & Mann, M. (2003). Stop and go extraction tips for matrix-assisted laser desorption/ionization, nanoelectrospray, and LC/MS sample pretreatment in proteomics. *Analytical Chemistry, 75*, 663–670.

Rappsilber, J., Mann, M., & Ishihama, Y. (2007). Protocol for micro-purification, enrichment, pre-fractionation and storage of peptides for proteomics using StageTips. *Nature Protocols, 2*, 1896–1906.

Saeed, A. I., Sharov, V., White, J., Li, J., Liang, W., Bhagabati, N., et al. (2003). TM4: A free, open-source system for microarray data management and analysis. *BioTechniques, 34*, 374–378.

Sakai, C., Tomitsuka, E., Esumi, H., Harada, S., & Kita, K. (2012). Mitochondrial fumarate reductase as a target of chemotherapy: From parasites to cancer cells. *Biochimica et Biophysica Acta, 1820*, 643–651.

Sugiyama, N., Masuda, T., Shinoda, K., Nakamura, A., Tomita, M., & Ishihama, Y. (2007). Phosphopeptide enrichment by aliphatic hydroxy acid-modified metal oxide chromatography for nano-LC-MS/MS in proteomics applications. *Molecular and Cellular Proteomics, 6*, 1103–1109.

Tomitsuka, E., Kita, K., & Esumi, H. (2010). The NADH-fumarate reductase system, a novel mitochondrial energy metabolism, is a new target for anticancer therapy in tumor microenvironments. *Annals of the New York Academy of Sciences, 1201*, 44–49.

Warburg, O. (1956). On the origin of cancer cells. *Science, 123*, 309–314.

Wiebe, M. G., Rintala, E., Tamminen, A., Simolin, H., Salusjarvi, L., Toivari, M., et al. (2008). Central carbon metabolism of *Saccharomyces cerevisiae* in anaerobic, oxygen-limited and fully aerobic steady-state conditions and following a shift to anaerobic conditions. *FEMS Yeast Research, 8*, 140–154.

Loss of HGF activator inhibits foveolar hyperplasia induced by oxyntic atrophy without altering gastrin levels

Yukinori Yamagata, Susumu Aikou, Tsuyoshi Fukushima, Hiroaki Kataoka, Yasuyuki Seto, Hiroyasu Esumi, Michio Kaminishi, James R. Goldenring and Sachiyo Nomura

Am J Physiol Gastrointest Liver Physiol 303:G1254-G1261, 2012. First published 11 October 2012; doi: 10.1152/ajpgi.00107.2012

Am J Physiol Gastrointest Liver Physiol 303: G1254–G1261, 2012.
First published October 11, 2012; doi:10.1152/ajpgi.00107.2012.

Loss of HGF activator inhibits foveolar hyperplasia induced by oxyntic atrophy without altering gastrin levels

Yukinori Yamagata (山形幸徳),[1] Susumu Aikou (愛甲丞),[1] Tsuyoshi Fukushima (福嶋剛),[2] Hiroaki Kataoka (片岡寛章),[2] Yasuyuki Seto (瀬戸泰之),[1] Hiroyasu Esumi (江角浩安),[3] Michio Kaminishi (上西紀夫),[4] James R. Goldenring,[5] and Sachiyo Nomura (野村幸世)[1]

[1]*Department of Gastrointestinal Surgery, Graduate School of Medicine, University of Tokyo, Tokyo, Japan;* [2]*Department of Pathology, Faculty of Medicine, University of Miyazaki, Miyazaki, Japan;* [3]*Research Center for Innovative Oncology, National Cancer Center Hospital East, Kashiwa, Japan;* [4]*Showa General Hospital, Kodaira, Japan; and* [5]*Nashville Veterans Affairs Medical Center and the Departments of Surgery and Cell and Developmental Biology, Epithelial Biology Center, Vanderbilt University School of Medicine, Nashville, Tennessee*

Submitted 15 March 2012; accepted in final form 8 October 2012

Yamagata Y, Aikou S, Fukushima T, Kataoka H, Seto Y, Esumi H, Kaminishi M, Goldenring JR, Nomura S. Loss of HGF activator inhibits foveolar hyperplasia induced by oxyntic atrophy without altering gastrin levels. *Am J Physiol Gastrointest Liver Physiol* 303: G1254–G1261, 2012. First published October 11, 2012; doi:10.1152/ajpgi.00107.2012.—Spasmolytic polypeptide/trefoil family factor 2 expressing metaplasia (SPEM) is induced by oxyntic atrophy and is known as a precancerous or paracancerous lesion. We now have sought to determine whether hepatocyte growth factor (HGF) influences the development of SPEM and oxyntic atrophy. DMP-777, a parietal cell ablating reagent, was administered to HGF activator (HGFA)-deficient mice and wild-type mice. Gastric mucosal lineage changes were analyzed in the DMP-777 treatment phase and recovery phase. Both wild-type and HGFA knockout mice showed SPEM, and there was no difference in SPEM development. However, after cessation of DMP-777, HGFA-deficient mice showed delayed recovery from SPEM compared with wild-type mice. Foveolar cell hyperplasia and the increase in proliferating cells after parietal cell loss were reduced in HGFA-deficient mice. The HGFA does not affect emergence of SPEM. However, the absence of HGFA signaling causes a delay in the recovery from SPEM to normal glandular composition. HGFA also promotes foveolar cell hyperplasia and mucosal cell proliferation in acute oxyntic injury.

metaplasia; gastric cancer; TFF2; HGF; SPEM

GASTRIC CANCER ARISES IN THE setting of atrophic gastritis caused by infection of *Helicobacter pylori* (*H. pylori*) (1, 23, 28). In the atrophic mucosa of the fundic glands of the stomach, spasmolytic polypeptide [trefoil family factor 2 (TFF2)] expressing metaplasia (SPEM), parietal cell loss, foveolar hyperplasia, as well as intestinal metaplasia, are observed. SPEM is associated with gastric cancer in the fundus at a higher rate than intestinal metaplasia and has been implicated as a precancerous lesion (4, 25, 29). The factors that can induce SPEM have not yet been identified, but several animal models produce SPEM, including mouse and rat *H. felis*/*H. pylori* infection models and administration of DMP-777 to mice and rats (3, 3a, 18, 19). DMP-777 is a cell-permeant neutrophil elastase inhibitor, which also acts as a parietal cell-specific protonophore and specifically ablates parietal cells. Treatment of mice with DMP-777 causes acute oxyntic atrophy, as well as foveolar hyperplasia, followed by the emergence of SPEM. Cessation of DMP-777 after administrating DMP-777 for 14 days leads to recovery of parietal cells, usually to a level greater than in untreated animals, and SPEM and foveolar hyperplasia resolve (19). In gastrin-deficient mice, compared with wild-type mice, SPEM appears earlier in response to DMP-777 administration and remains later after termination of drug treatment (19), even though hypergastrinemia accompanies atrophic gastritis in wild-type mice (9, 17).

Recent investigations have increasingly suggested that hepatocyte growth factor (HGF) plays an important role in the ontogeny and restoration of the gastrointestinal epithelium (8, 27). C-Met, which is the receptor for HGF, is overexpressed in gastric cancer, and HGF is implicated in gastric carcinogenesis. HGF was discovered in 1984 as the bioactive substance, which promoted the production and the expansion of hepatocytes (14). HGF was also identified as "scatter factor" (26), which controls scattering of kidney cells. HGF is secreted as an inactive single-chain form by mesenchymal cells and, following limited degradation by a serine protease, is converted into its activated two-chain form (15). Activated HGF acts as a mitogen, a motogen, and a morphagen for various cell lineages, including epithelial cells and inner skin cells through its receptor, c-Met tyrosine kinase (13, 14, 26). In the gastrointestinal mucosa, HGF is activated only in damaged lesions (11), and the efficiency of HGF activation is important for proliferation and restoration in the damaged mucosa.

HGF activator (HGFA), which resembles coagulation factor XII, is a serine protease, which is one of the most efficient activators of HGF. Other proteases, such as urokinase, tissue-type plasminogen activator, factor XII, factor XI, plasma kallikrein, matriptase, and hepsin can activate HGF in vitro. The latter two are transmembrane serine proteases, whereas the other five proteases originate from the plasma. All of these proteases are very weak activators of HGF, compared with HGFA, in vitro (12). HGFA is produced in the liver as an inactive protein form that is abundantly secreted into the circulation. In damaged organs, HGFA is activated by activated thrombin, degraded by kallikrein, and becomes a 34-kDa two-chain form (8). In the early stages of mucosal injury, HGFA is activated in damaged mucosa and promotes activation of HGF, which participates in mucous membrane restoration. Mucosal repair is impaired in the HGFA-deficient mouse, as HGF activation in the damaged legion is reduced by the lack of HGFA (7).

Address for reprint requests and other correspondence: S. Nomura, Dept. of Gastrointestinal Surgery, Graduate School of Medicine, Univ. of Tokyo, 7-3-1 Hongo, Bunkyo-ku, Tokyo 113-8655, Japan (e-mail: snomura-gi@umin.ac.jp).

The purpose of this study was to examine the participation of HGF in the generation of SPEM after loss of gastric parietal cells (acute oxyntic atrophy). Since HGF deficiency in mice is embryonic lethal, we employed the HGFA-deficient mouse model. We examined the changes in the gastric mucosal cell lineages of the HGFA-deficient mice when DMP-777 was administered compared with the changes in wild-type mice.

MATERIALS AND METHODS

Materials. DMP-777, formulated at a concentration of 2% as a suspension in 0.5% methylcellulose, was a gift of DuPont Pharmaceuticals. 5-Bromo-2′-deoxyuridine (BrdU) was obtained from Sigma.

Animals. C57BL/6 mice were obtained from Charles River Breeding Laboratories. HGFA-deficient mice were made as previously described (7). During the experiments, mice were kept in cages provided with water and regular chow ad libitum until the time of death. All animal experimental procedures were reviewed and approved by the Institutional Animal Care and Research Advisory Committee of the University of Tokyo.

Study design. Male C57BL/6 wild-type control mice (8 wk of age) and male HGFA-deficient mice (8 wk of age) were administrated DMP-777 by oral gavage (350 mg/kg) once daily. Groups of six mice were killed before starting drug administration and after 1, 3, 7, 10, and 14 days of drug administration. Additionally, groups of three to eight mice, which received 14 days of drug administration, were killed 7 (R7), 14 (R14), and 28 (R28) days after cessation of 14-day drug administration.

Necropsy and tissue processing. BrdU in saline (200 mg/kg) was injected intraperitoneally in all mice 2 h before necropsy. Each mouse was anesthetized with avertin and was perfused through the left ventricle with PBS (pH 7.4) for 1 min, followed by 4% paraformaldehyde for 10 min. Each stomach was excised and opened along the greater curvature, then cut into 2-mm-wide strips parallel to the lesser curvature and embedded in paraffin. For histological studies, 5-μm sections were prepared.

For RNA extraction, the mice were killed by CO_2 inhalation, and the fundic regions of stomachs were excised, snap frozen with liquid nitrogen, and kept in −80°C until use.

Histological examination. We performed histochemistry and immunohistochemistry to explore the alterations in the gastric fundic mucosa. Histochemistry was performed for diastase-resistant periodic acid Schiff (DR-PAS) to detect surface mucous cells.

Murine monoclonal anti-H-K-ATPase IgG (a gift from Dr. Adam Smolka, Medical University of South Carolina, Charleston, SC), murine monoclonal anti-human TFF2 IgM (a gift from Dr. Nicholas Wright, Cancer UK, London, UK), and rabbit polyclonal anti-human intrinsic factor (IF) (a gift from Dr. David Alpers, Washington University, St. Louis, MO) were used as markers to identify parietal cells, mucous neck cells, and chief cells in fundic glands, respectively. For immunohistochemistry of anti-H-K-ATPase and anti-TFF2, deparaffinized sections were blocked using blocking serum provided in the HistoMouse staining kit (Zymed, South San Francisco, CA). Sections were incubated with a primary antibody (1:1,000 and 1:100 for anti-H-K-ATPase and anti-human TFF2, respectively) overnight at 4°C. Indirect immunohistochemical detection was then performed through incubation with biotinylated secondary antibodies and alkaline phosphatase-conjugated streptavidin (Vectastain ABC KIT, Vector Laboratories, Burlingame, CA). Chromogen was developed with Vector Red (Vector Laboratories).

For immunohistochemistry with anti-IF, deparaffinized sections were blocked with 1.5% normal goat serum and incubated with the primary antibody (1:1,000) overnight at 4°C, followed by incubation with a biotinylated second antibody and alkaline phosphatase-conjugated streptavidin. Chromogen was developed with Vector Red.

For immunohistochemistry of BrdU, a BrdU staining kit (Zymed) was used following the recommended instructions. In brief, sections were incubated in 0.25% trypsin for 2 min, followed by blocking of endogenous peroxidase activity with 3% H_2O_2. After incubation with a blocking serum, sections were incubated with biotinylated murine monoclonal anti-BrdU overnight at 4°C, followed by incubation with

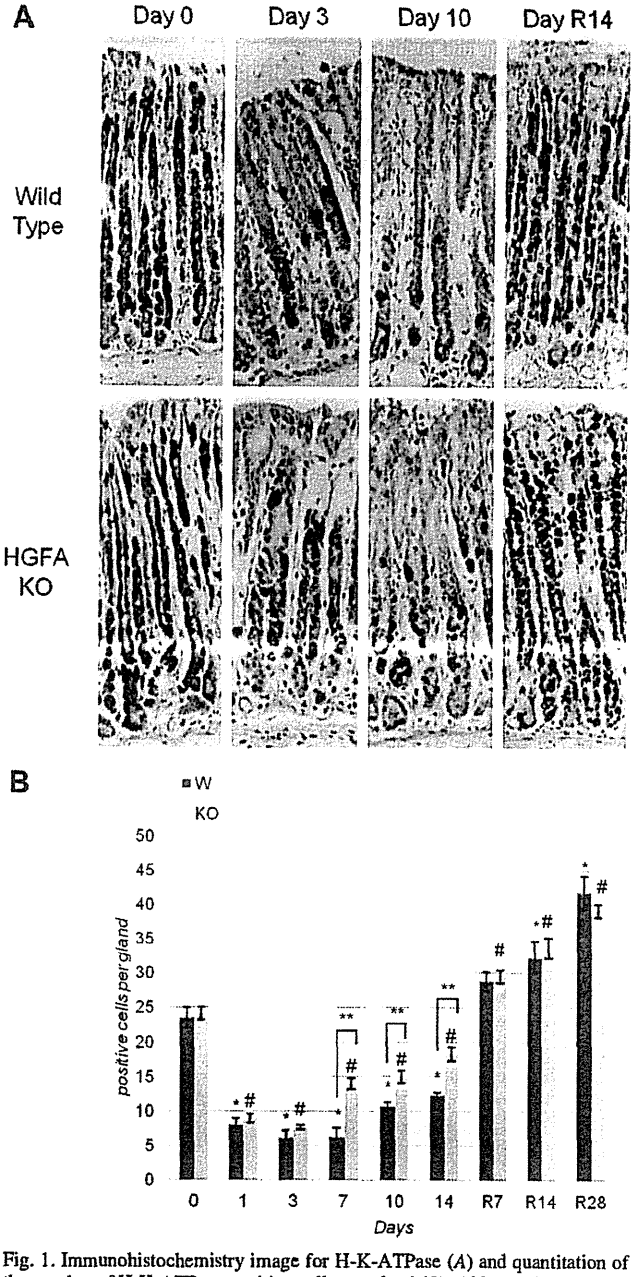

Fig. 1. Immunohistochemistry image for H-K-ATPase (*A*) and quantitation of the number of H-K-ATPase-positive cells per gland (*B*). Although both groups showed a significant reduction in the number of H-K-ATPase-positive cells at *day 3* of treatment, after recovery *day 7* (*day R7*), they recovered to the same level as untreated mice, and an overshoot was observed. Significant difference was observed on *days 7–14*. Numbers at each time point were compared with *day 0* by Dunnett's test. $*P < 0.05$ for wild-type (W) mice. $\#P < 0.05$ for knockout (KO) mice. Numbers for wild-type and KO mice at each time point were compared by Student's *t*-test. $**P < 0.05$. Values are means ± SE. HGFA, hepatocyte growth factor (HGF) activator.

horseradish peroxidase-conjugated streptavidin. Chromogen was developed with diaminobenzidine.

For immunostaining of activated c-Met, anti-phosphorylated (Y1235) human c-Met rabbit polyclonal antibody, which cross-reacts with mouse phosphorylated (Y1233) c-Met (6), was used. For immunostaining of HGF, rabbit polyclonal antibody raised against the amino-terminal amino acid sequence of HGF α-chain (IBL, Fujioka, Japan) was used. Immunohistochemical detection was performed according to the method described previously (6).

For all immunostaining, the sections were counterstained with Gill's hematoxylin and mounted.

TUNEL method. For analysis of HGF effect on apoptosis, the terminal deoxynucleotidyl transferase-mediated dUTP nick end labeling (TUNEL) method was applied. Apoalert DNA Fragmentation Assay Kit (Takara Bio, Otsu) was used according to the manufacturer's instructions.

Quantitation of cell lineages. Ten well-oriented glands were chosen from sections of the posterior wall of the fundic area of each stomach. The number of stained cells was determined, and the number of positive cells for each gland unit was calculated (visualized at ×200).

RT-PCR for HGF. Frozen fundic regions of the stomach were homogenized in ISOGEN-LS (Nippongene, Toyama), and total RNA was extracted according to the manufacturer's instructions. One microgram of total RNA was mixed with 0.25 μg of random primer (Promega, Tokyo) and incubated at 70°C for 10 min. Then first-strand buffer, dNTP mix, DTT, and Powerscript RT (Clontech, Otsu) were added and incubated at 42°C for 90 min. The reaction was terminated by heating at 70°C for 15 min.

Quantitative PCR was performed with an Eco real-time PCR system (Illumina, Tokyo), using MESA GREEN qPCR master mix plus for SYBR (EUROGENTEC, Toyama) as in the manufacturer's instructions. The PCR was performed with 40 cycles of 95°C for 1

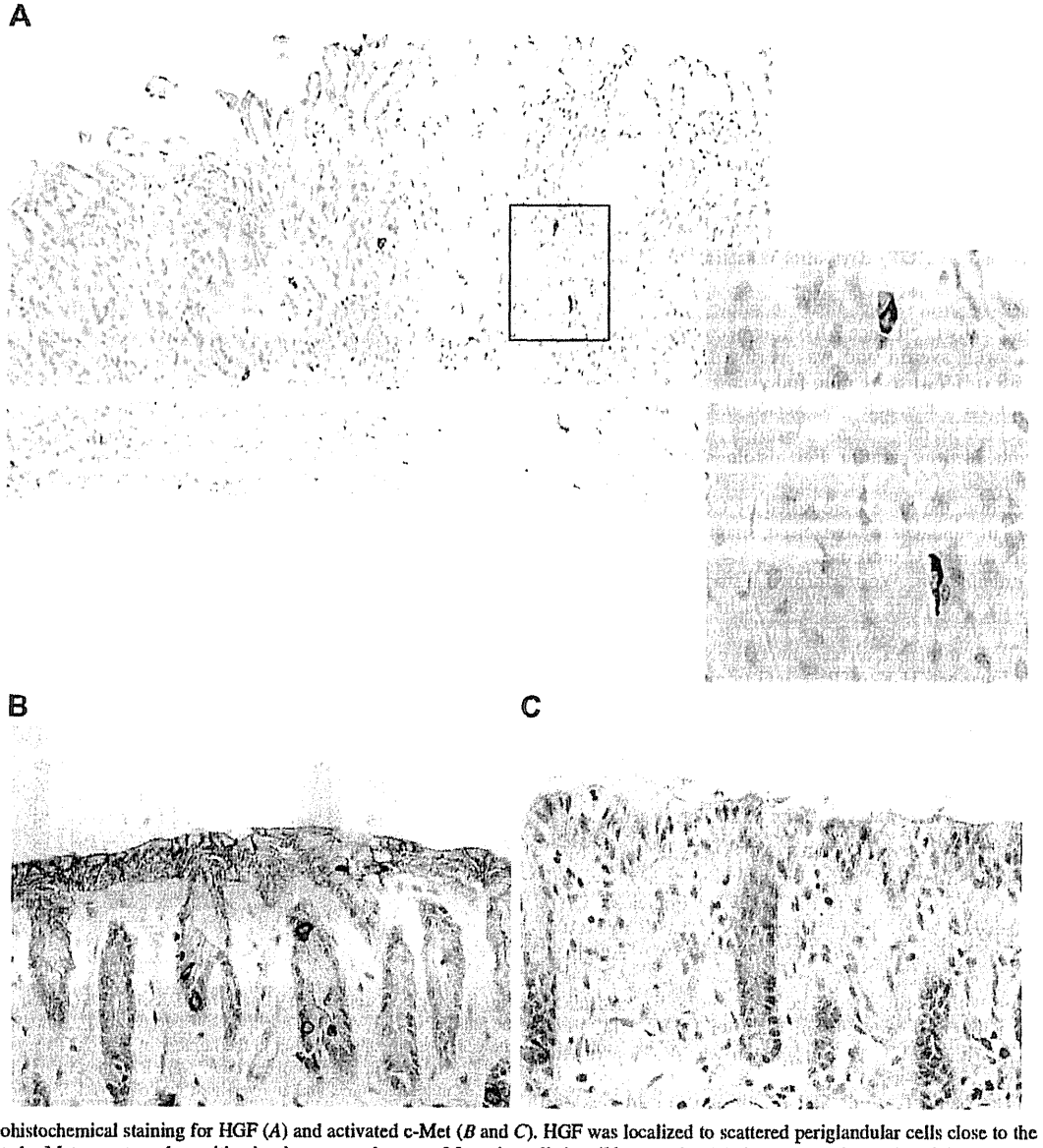

Fig. 2. Immunohistochemical staining for HGF (*A*) and activated c-Met (*B* and *C*). HGF was localized to scattered periglandular cells close to the middle of the glands. Activated c-Met was strongly positive in plasma membranes of foveolar cells in wild-type mice (*B*); however, only weak staining was present in HGFA KO mice (*C*). Some strongly stained cells were observed in the neck region of fundic glands of wild-type mice. The identity of these cells is unknown.

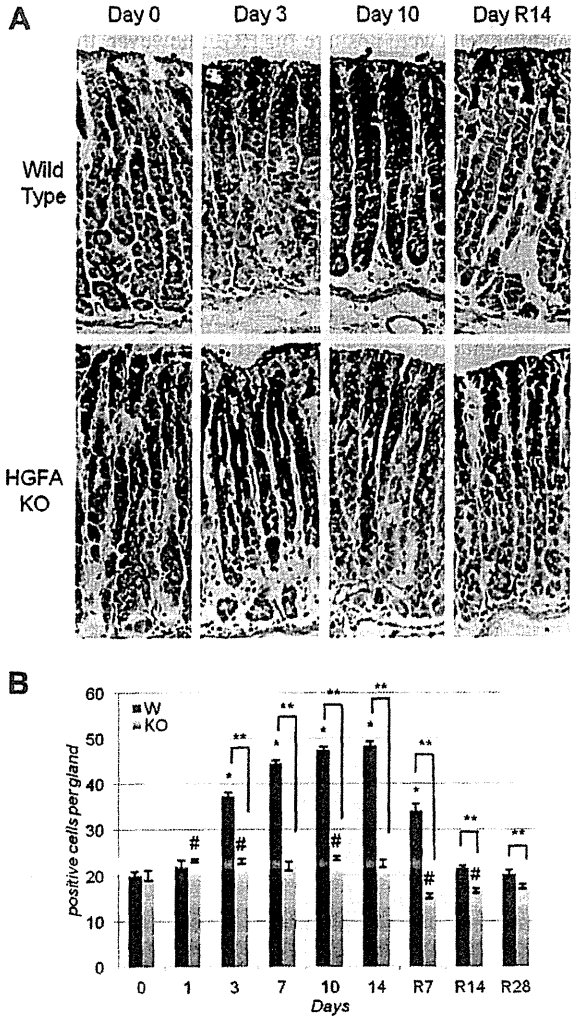

Fig. 3. Histochemistry for diastase-resistant periodic acid Schiff (DR-PAS) staining (*A*) and the quantitated changes in the number of DR-PAS-positive cells per gland (*B*). Although a remarkable increase in the number of DR-PAS-positive cells was observed after *day 3* in wild-type mice, these changes were not observed in HGFA KO mice. Foveolar cell numbers recovered to the untreated level in wild-type mice and were lower than original level in KO mice after *day R7*. After *day 3*, the number of DR-PAS-positive cells was significantly lower in KO mice compared with wild type. Numbers at each time point were compared with *day 0* by Dunnett's test. $*P < 0.05$ for wild type. $\#P < 0.05$ for KO mice. Numbers in wild-type and KO mice at each time point were compared by Student's *t*-test. $**P < 0.05$. Values are means ± SE.

min, 60°C for 30 s, and 72°C for 20 s. The forward primer for the control GAPDH was CGTCCCGTAGACAAAATGGT, the reverse primer for GAPDH was AATTTGCCGTGAGTGGAGTC, the forward primer for HGF was TTCCCAGCTGGTCTATGGTC and the reverse primer for HGF was TGGTGCTGACTGCATTTCTC.

Measurement of serum gastrin levels. Blood gathered from the right atrium of the mouse was centrifuged at 3,000 rpm for 10 min, and the supernatant was collected and saved at −80°C until use. The serum gastrin levels were measured by radioimmunoassay by SRL (Tachikawa, Tokyo).

Statistical analysis. All statistical analyses were performed using JMP7 software. The number of cells and the serum gastrin levels were evaluated by ANOVA, Dunnett test, and Student's *t*-test. Dunnett test was used for comparison of the value of each time point to the value of *day 0* in each mouse group. Student's *t*-test was performed when the values of wild-type and HGFA knockout (KO) mice were compared at each time point. *P* values < 0.05 were considered statistically significant.

RESULTS

Parietal cell loss induced by DMP-777. The cells immunoreactive for the α-subunit of H-K-ATPase were counted as parietal cells. Figure 1*A* shows representative pictures of immunostaining for H-K-ATPase, and Fig. 1*B* shows the number of H-K-ATPase-positive cells per gland. One day after DMP-777 administration, the number of H-K-ATPase-positive cells decreased to 33–37% of untreated mice in both wild-type and HGFA-deficient mice, and, after 3 days of treatment, the number decreased to 26–32%. The number of parietal cells was reduced throughout DMP-777 treatment. However, as previously reported,

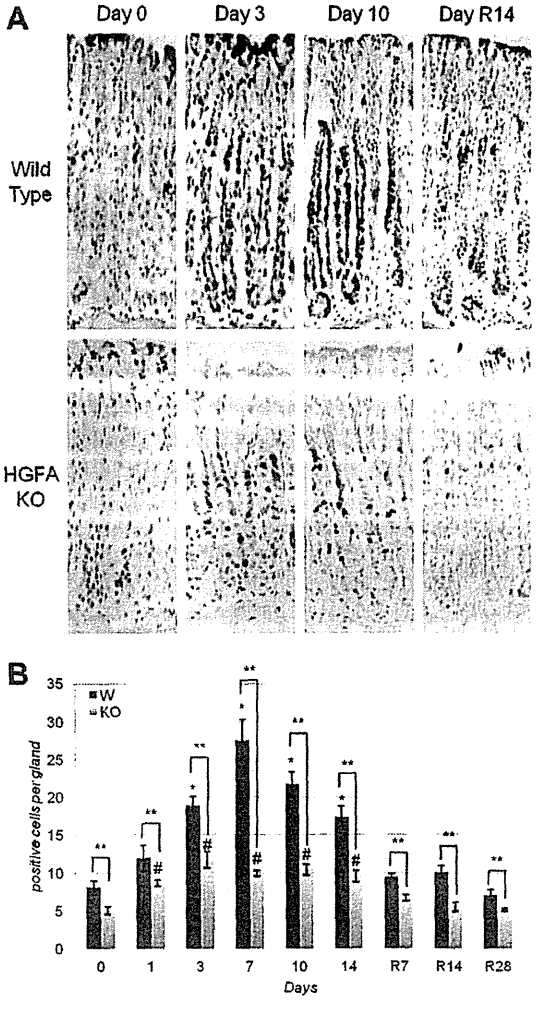

Fig. 4. Immunohistochemical staining for 5-bromo-2′-deoxyuridine (BrdU; *A*) and quantitation of the number of BrdU-positive cells per gland (*B*). In both groups, the number of BrdU-positive cells significantly increased after *day 3* and returned to the untreated level by *day R7*. The number of BrdU-positive cells was significantly lower in KO mice than in wild-type mice at all time points. Numbers at each time point were compared with *day 0* by Dunnett's test. $*P < 0.05$ for wild type. $\#P < 0.05$ for KO. Numbers in wild-type and KO mice at the same time point were compared by Student's *t*-test. $**P < 0.05$. Values are means ± SE.

after 7 days of treatment, we did observe some recovery of parietal cells. This recovery was complete and reached levels greater than in untreated mice after R7 and R14 days off of drug treatment. An increase of 23–78% was observed at *days R7*, *R14*, and *R28* compared with the level before administration. The number of H-K-ATPase-positive cells in the HGFA KO group was significantly greater than that of wild-type group 7–14 days after beginning the DMP-777 administration, but, in the recovery phase after withdrawal of DMP-777 treatment, recovery of H-K-ATPase-positive cells was equivalent. The number of H-K-ATPase-positive cells after DMP-777 administration in both groups increased with time of recovery, with R7 < R14 < R28. The overshoot of parietal cell numbers was maintained at least until R28 in both groups.

HGF activation after acute parietal cell loss. To confirm that the origin of HGF is not parietal cells, we examined the immunolocalization of HGF and quantitative RT-PCR for HGF before and after administration of DMP-777. By quantitative RT-PCR, in wild-type mice there was no difference in HGF mRNA expression in the fundic mucosa comparing untreated mice and mice treated with DMP-777 for 10 days (data not shown). HGF immunostaining is shown in Fig. 2*A*. Several periglandular cells were positive for HGF; however, there was no detectable staining in parietal cells.

To assess the HGF activation in wild-type mice and HGFA KO mice, activated c-Met immunostaining was performed. As shown in Fig. 2*B*, activated c-Met was strongly positive in cell membranes of foveolar cells and in some cells in the neck region, but only in wild-type mice (Fig. 2*C*). Foveolar cell membranes of HGFA KO mice demonstrated only weak staining for activated c-Met.

Foveolar cell numbers after acute parietal cell loss. We utilized DR-PAS histochemistry to stain foveolar cells. Figure 3*A* shows representative staining for DR-PAS, and Fig. 3*B* shows the changes in the number of foveolar cells per gland. In untreated mice, the number of DR-PAS-positive cells in wild-type and HGFA-deficient mice was equivalent. A significant foveolar cell hyperplasia was observed only in wild-type mice. After 3 days of DMP-777 administration and after 14 days of treatment, the number of DR-PAS-positive cells increased 2.4-fold over the numbers in untreated mice. On the other hand, in HGFA KO mice, although there was a statistically

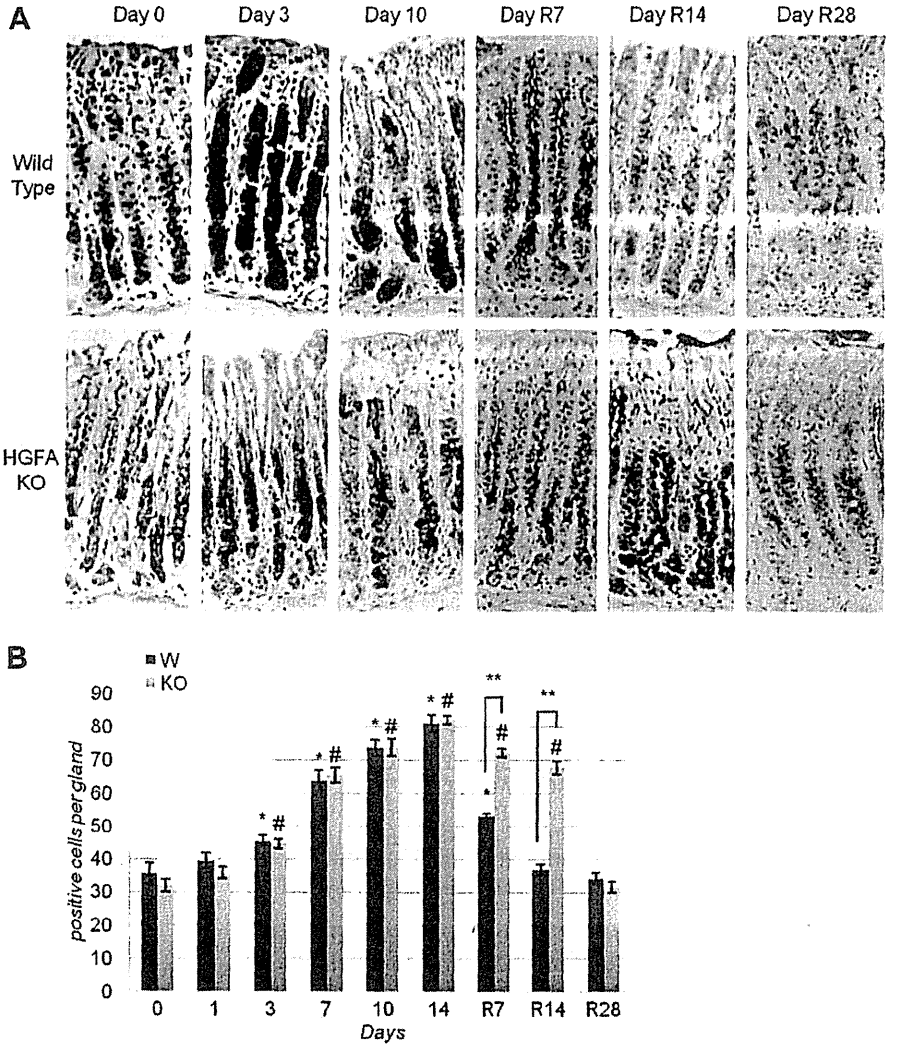

Fig. 5. Immunohistochemical staining for trefoil family factor 2 (TFF2; *A*) and the quantitation of the changes in the numbers of TFF2-positive cells per gland (*B*). Numbers of TFF2-positive cells in wild type and KO are similar on *days 0–14*. In KO mice, the number of TFF2-positive cells was significantly higher compared with wild type at *days R7* and *R14*. Recovery from spasmolytic polypeptide/TFF2 expressing metaplasia to normal glands was slower in KO mice. Numbers at each time point were compared with *day 0* by Dunnett's test. $*P < 0.05$ for wild type. $\#P < 0.05$ for KO mice. Numbers of wild-type and KO mice were compared at each same time point by Student's *t*-test. $**P < 0.05$. Values are means ± SE.

significant increase in foveolar cells compared with *day 0*, the increase was much reduced (10–18%) compared with the changes in wild-type mice. By *day R14*, the number of DR-PAS-positive cells returned to its initial level in wild-type mice and showed a small decrease in HGFA KO mice. Comparing both groups, the number of foveolar cells in HGFA KO mice was significantly smaller than that in wild-type mice, from *day 3* of DMP-777 treatment through *day R28*.

Effects of acute parietal loss on S-phase proliferating cells. BrdU staining was used to assess S-phase proliferating cell lineages. Figure 4*A* shows representative immunohistochemistry images of BrdU staining, and Fig. 4*B* displays the changes in the number of BrdU-positive cells per gland. Both groups showed increased numbers of proliferating cells beginning 1 day after DMP-777 administration. The increases in proliferation peaked at 2.0- to 3.4-fold at *day 7* and then declined afterwards. Proliferation in both groups returned to the untreated levels by *day R7*. HGFA KO mouse stomachs showed significantly fewer BrdU-positive cells throughout the whole period compared with wild-type mice.

Alterations in TFF2-positive cells and induction of SPEM in response to parietal cell loss. Figure 5*A* shows representative figures of immunohistochemical staining of TFF2, and Fig. 5*B* shows the changes in the numbers of TFF2-positive cells per gland. In the normal fundic glands in untreated mice, TFF2 stained in mucous neck cells, which are located in the middle third of the gland. Before DMP-777 administration, TFF2-positive cells resided around the middle of the gland in both wild-type and HGFA KO mice, and the number of TFF2-positive cell was equivalent in both types. The number of TFF2-positive cells began to increase significantly from *day 3* of DMP-777 administration and continued to rise until *day 14* of treatment, with appearance of SPEM expanding from the bases of glands. Although there was no difference between groups during DMP-777 administration, at *days R7* and *R14*, the number of TFF2-positive cells in HGFA KO mice remained significantly higher than in untreated mice, while the numbers TFF2-immunoreactive cells in wild-type mice returned to the level in untreated mice by *day R14*. In comparison between both groups, the number of TFF2-positive cells in HGFA KO was significantly higher than in wild-type mice at *days R7* and *R14*. These results indicate that the loss of SPEM following removal of DMP-777 in HGFA KO mice was delayed compared with that in wild-type mice. On *day R28*, the number of TFF2-positive cells returned to the same level as *day 0* in both groups of mice.

Effects of oxyntic atrophy of expression of IF. The immunohistochemical staining of IF was used as a maker of chief cells. Figure 6*A* shows representative figures of immunohistochemical staining of IF, and Fig. 6*B* shows the changes in the numbers of IF-positive cells per gland. We observed a small decrease in the number of IF-positive cells on *days 3–14* of treatment (wild-type 10–25% and HGFA KO 2–10% decrease), although neither change was statistically significant. In *days R7–R28* mice, the number of IF-positive cells recovered to the untreated levels in both groups.

Effects of oxyntic atrophy on apoptosis. Apoptosis was assessed by the TUNEL method. As shown in Fig. 7*A*, TUNEL-positive cells were localized to foveolar cells close to the mucosal surface. Apoptotic cell numbers were much higher in wild-type mice than in HGFA KO mice without treatment (Fig. 7*B*). After DMP-777 treatment, apoptotic cell numbers decreased significantly compared with untreated mice only in wild-type mice from *day 1* to *day R7*. No change in apoptotic cell numbers was observed in HGFA KO mice throughout the treatment period. On *days 0, R14*, and *R28*, the apoptotic cell number was significantly higher in wild-type mice compared with HGFA KO mice.

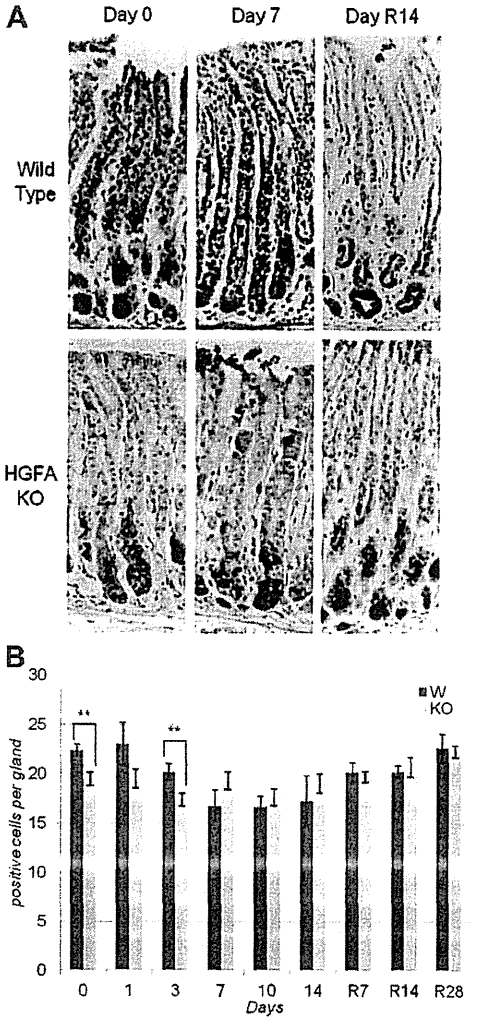

Fig. 6. Immunohistochemical staining for intrinsic factor (IF; *A*) and the quantitation of the changes in the numbers of IF-positive cells per gland (*B*). Although there was a tendency for decreasing numbers of IF-positive cells during DMP-777 treatment, there was no significant difference from the original number in either group. Numbers at each time point were compared with *day 0* by Dunnett's test. $^{**}P < 0.05$. Values are means ± SE.

Serum gastrin levels after induction of oxyntic atrophy. Our laboratory has previously reported that the hyperplasia of foveolar cells after DMP-777 treatment depended on an increase in gastrin, as exemplified by the absence of foveolar hyperplasia in gastrin-deficient mice treated with DMP-777 (10). Because the change in the number of foveolar cells was significantly different between wild-type and HGFA KO in these studies, we measured serum gastrin level.

Figure 8 shows the changes of serum gastrin levels. Both groups showed a significant rise of the serum gastrin level on *days 1–14* of DMP-777 treatment. The serum gastrin levels dropped on *day 14*, but were still elevated compared with the level on *day 0*.

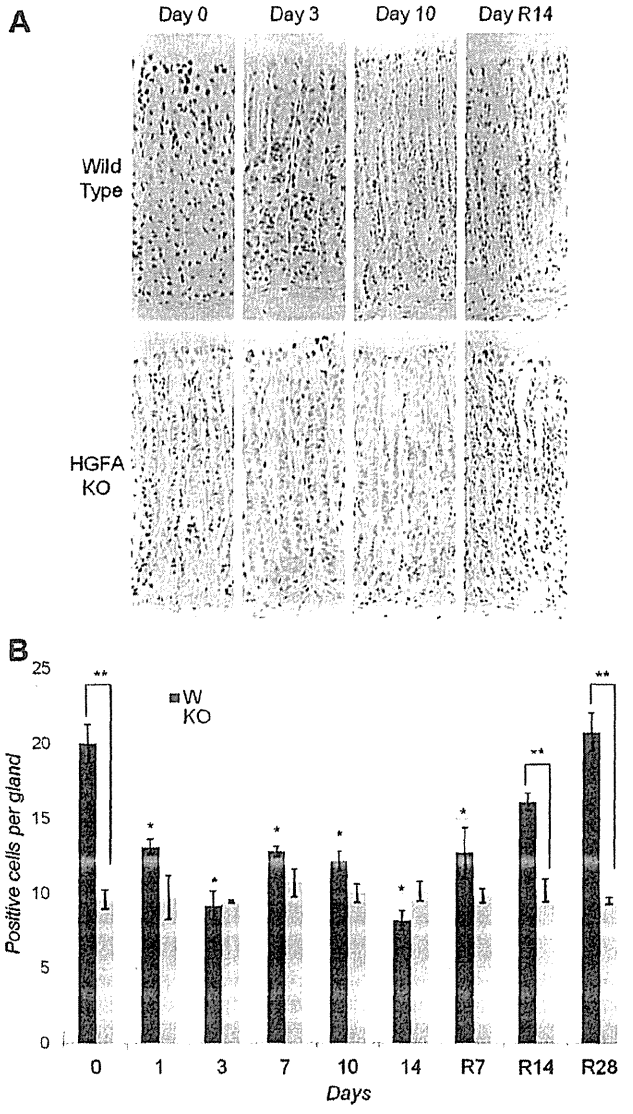

Fig. 7. Terminal deoxynucleotidyl transferase-mediated dUTP nick end labeling (TUNEL) staining in wild-type and HGFA KO mice (*A*) and quantitation of the numbers of apoptotic cells per gland (*B*). TUNEL-positive cells were localized to foveolar cells close to the surface of mucosa. The number of TUNEL-positive cells was much higher in wild-type mice compared with HGFA KO mice. DMP-777 administration caused a reduction in the number of TUNEL-positive cells to a level similar to that in HGFA KO mice. The number of TUNEL-positive cells was not changed by DMP-777 administration in HGFA KO mice. $*P < 0.05$ in wild type. $**P < 0.05$. Values are means ± SE.

DISCUSSION

Gastric cancer arises in the setting of atrophic gastritis, which is accompanied by foveolar cell hyperplasia and SPEM formation. In this study, foveolar cell hyperplasia was observed in wild-type mice following DMP-777-induced parietal cell loss, but was not observed in HGFA-deficient mouse after induction of oxyntic atrophy. These findings suggest that HGF is needed for foveolar cell hyperplasia formation in atrophic gastritis. In support of this, activated c-Met was positive in the plasma membranes of foveolar cells only in wild-type mice and was absent in HGFA KO mice. HGF is activated in the gastric mucosa by activated HGFA when the mucosa is damaged, and foveolar hyperplasia is one of the defensive changes in the gastric mucosa (8, 13, 21, 22). Our laboratory has reported previously that foveolar cell hyperplasia was not observed in gastrin-deficient mouse following DMP-777 administration (19). In the present studies, the serum gastrin levels were elevated in HGFA-deficient mice after DMP-777 treatment to the same extent as seen in wild-type mice through 10 days of administration. Nevertheless, foveolar cell hyperplasia was essentially absent in DMP-777-treated HGFA-deficient mice. These results indicate that both HGF and gastrin are needed for induction of foveolar cell hyperplasia, and that induction of HGF activation must lie downstream of, or be permissive for, gastrin stimulation of foveolar cell production. In support of this concept, HGF is induced by the gastrin stimulation in cultured gastric cancer cells (10). How gastrin stimulation leads to HGF activation and foveolar cell hyperplasia remains to be determined in the future.

In untreated mice, the number of both BrdU-positive cells and apoptotic cells were higher in wild-type mice compared with HGFA KO mice. As there was no difference in the number of mucosal cell lineages in both mice, cell proliferation and apoptosis are balanced in HGFA KO mice by hypoproliferation and hypoapoptosis. Although an increase in BrdU-positive cells was observed during the DMP-777 dosing period in both groups, we observed a smaller increase in HGFA-deficient mice compared with wild-type mice. Apoptotic cell number was dramatically reduced in wild-type mice during the DMP-777 dosing period, but no changes were found in HGFA KO mice. Foveolar hyperplasia can result from hyperproliferation in the neck of the fundic glands, as well as from reduction of apoptosis in foveolar cells in wild-type mice. Thus HGF likely promotes both cell proliferation and apoptosis in the normal gastric mucosa, and further increases cell proliferation without promoting apoptosis in the atrophic mucosa. In atrophic gastritis, HGF promote tumor growth and cell proliferation and anti-apoptosis.

Our laboratory has reported that "transdifferentiation" of chief cells, expressing IF, accounts for the origin of SPEM (2, 16, 20). In the normal fundic gland, mucous neck cells migrate toward the bottom of the gland and, at the same time, differentiate into the chief cell. In generating SPEM, our laboratory has reported that

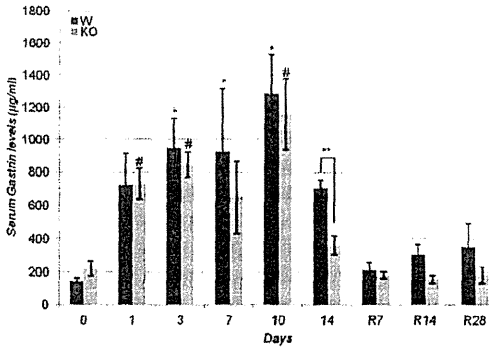

Fig. 8. Serum gastrin levels in wild-type and HGFA KO mice. Serum gastrin levels in both groups increased on *day 1* of DMP-777 treatment and remained elevated until *day 10*. On *day 14*, the level of both groups decreased. In comparisons between the groups, a significant difference was observed only on *day 14*. Numbers at each time point were compared with *day 0* by Dunnett's test. $*P < 0.05$ in wild type. $\#P < 0.05$ in KO. Numbers in wild-type and KO mice at the same time point are compared by Student's *t*-test. $**P < 0.05$. Values are means ± SE.

the mature chief cell transdifferentiates into TFF2-expressing SPEM cells in the setting of acute oxyntic atrophy (2, 16, 20). In this experiment, the emergence of SPEM and the change in the number of TFF2-positive cells were equivalent in both wild-type and HGFA-deficient mice, even though the increase of BrdU-positive cells was smaller in HGFA-deficient mice. This result supports the concept that the origin of SPEM following DMP-777 treatment is predominantly due to "transdifferentiation" rather than activation of a cryptic proliferative cell population.

The association of SPEM with gastric cancer in humans suggests that SPEM may be a precancerous lesion. Because it was reported that HGF contributed to the development of gastric cancer (5, 6), it seemed possible that SPEM formation would be promoted by HGF. However, no difference in SPEM formation following acute oxyntic atrophy was observed in HGFA-deficient mice, even though parietal cell numbers were slightly higher in HGFA-deficient mice from *day 7* through *day 14*. On the other hand, after the end of DMP-777 administration, a delay in the recovery from SPEM back to a normal mucosa was observed in HGFA-deficient mouse. Thus HGF and HGFA do appear to contribute to the recovery of the damaged mucosa from SPEM to normal lineages. These results support the concept that HGF and HGFA promote normal cell differentiation in the gastric fundic mucosa. Thus loss of HGFA prevents gastrin-stimulated foveolar hyperplasia and delays the normal recovery from oxyntic atrophy.

ACKNOWLEDGMENTS

We thank Miki Furuya for technical assistance. We also thank Dr. Nicholas Wright, Dr. Adam Smolka, and Dr. David Alpers for kind gifts of antibodies.

DISCLOSURES

No conflicts of interest, financial or otherwise, are declared by the author(s).

AUTHOR CONTRIBUTIONS

Author contributions: Y.Y., S.A., and T.F. performed experiments; Y.Y. and S.N. analyzed data; Y.Y. prepared figures; Y.Y. drafted manuscript; Y.Y., S.A., T.F., H.K., Y.S., H.E., M.K., J.R.G., and S.N. approved final version of manuscript; H.K., Y.S., H.E., M.K., J.R.G., and S.N. interpreted results of experiments; J.R.G. and S.N. conception and design of research; J.R.G. and S.N. edited and revised manuscript.

REFERENCES

1. **[Anon].** Schistosomes, liver flukes, and *Helicobacter pylori*. IARC Working Group on the Evaluation of Carcinogenic Risks to Humans. Lyon, 7–14 June 1994. *IARC Monogr Eval Carcinog Risks Hum* 61: 1–241, 1994.
2. **Goldenring JR, Nomura S.** Differentiation of the gastric mucosa III. Animal models of oxyntic atrophy and metaplasia. *Am J Physiol Gastrointest Liver Physiol* 291: G999–G1004, 2006.
3. **Goldenring JR, Poulsom R, Ray GS, Wright N, Meise KS, Coffey RJ Jr.** Expression of trefoil peptides in the gastric mucosa of transgenic mice overexpressing transforming growth factor-alpha. *Growth Factors* 13: 111–119, 1996.

3a. **Goldenring JR, Ray GS, Coffey RJ, Meunier PC, Haley PJ, Barnes TB, Car BD.** Reversible drug-induced oxyntic atrophy in rats. *Gastroenterology* 118: 1080–1093, 2000.

4. **Halldorsdottir AM, Sigurdardottrir M, Jonasson JG, Oddsdóttir M, Magnússon J, Lee JR, Goldenring JR.** Spasmolytic polypeptide-expressing metaplasia (SPEM) associated with gastric cancer in Iceland. *Dig Dis Sci* 48: 431–441, 2003.
5. **Han SU, Lee JH, Kim WH, Cho YK, Kim MW.** Significant correlation between serum level of hepatocyte growth factor and progression of gastric carcinoma. *World J Surg* 23: 1176–1180, 1999.
6. **Inoue T, Kataoka H, Goto K, Nagaike K, Igami K, Naka D, Kitamura N, Miyazawa K.** Activation of c-Met (hepatocyte growth factor receptor) in human gastric cancer tissue. *Cancer Sci* 95: 803–808, 2004.
7. **Itoh H, Naganuma S, Takeda N, Miyata S, Uchinokura S, Fukushima T, Uchiyama S, Tanaka H, Nagaike K, Shimomura T, Miyazawa K, Yamada G, Kitamura N, Koono M, Kataoka H.** Regeneration of injured intestinal mucosa is impaired in hepatocyte growth factor activator-deficient mice. *Gastroenterology* 127: 1423–435, 2004.
8. **Kataoka H, Miyata S, Uchinokura S, Itoh H.** Roles of hepatocyte growth factor (HGF) activator and HGF activator inhibitor in the pericellular activation of HGF/scatter factor. *Cancer Metastasis Rev* 22: 223–236, 2003.
9. **Konda Y, Kamimura H, Yokota H, Hayashi N, Sugano K, Takeuchi T.** Gastrin stimulates the growth of gastric pit with less-differentiated features. *Am J Physiol Gastrointest Liver Physiol* 277: G773–G784, 1999.
10. **Konturek PC, Kania J, Kukharsky V, Ocker S, Hahn EG, Konturek SJ.** Influence of gastrin on the expression of cyclooxygenase-2, hepatocyte growth factor and apoptosis-related proteins in gastric epithelial cells. *J Physiol Pharmacol* 54: 17–32, 2003.
11. **Miyazawa K, Shimomura T, Naka D, Kitamura N.** Proteolytic activation of hepatocyte growth factor in response to tissue injury. *J Biol Chem* 269: 8966–8970, 1994.
12. **Miyazawa K.** Hepatocyte growth factor activator (HGFA): a serine protease that links tissue injury to activation of hepatocyte growth factor. *FEBS J* 277: 2208–2214, 2010.
13. **Montesano R, Matsumoto K, Nakamura T, Orci L.** Identification of a fibroblast-derived epithelial morphogen as hepatocyte growth factor. *Cell* 67: 901–908, 1991.
14. **Nakamura T, Nawa K, Ichihara A.** Partial purification and characterization of hepatocyte growth factor from serum of hepatectomized rats. *Biochem Biophys Res Commun* 122: 1450–1459, 1984.
15. **Nakamura T, Nishizawa T, Hagiya M, Seki T, Shimonishi M, Sugimura A, Tashiro K, Shimizu S.** Molecular cloning and expression of human hepatocyte growth factor. *Nature* 342: 440–443, 1989.
16. **Nam KT, Lee HJ, Sousa JF, Weis VG, O'Neal RL, Finke PE, Romero-Gallo J, Shi G, Mills JC, Peek RM Jr, Konieczny SF, Goldenring JR.** Mature chief cells are cryptic progenitors for metaplasia in the stomach. *Gastroenterology* 139: 2028–2037, 2010.
17. **Neuburger P, Lewin M, de Recherche C, Bonfils S.** Parietal and chief cell populations in four cases of the Zollinger-Ellison syndrome. *Gastroenterology* 63: 937–942, 1972.
18. **Nomura S, Baxter T, Yamaguchi H, Leys C, Vartapetian AB, Fox JG, Lee3 JR, Wang TC, Goldenring JR.** Spasmolytic polypeptide expressing metaplasia to preneoplasia in *H. felis*-infected mice. *Gastroenterology* 127: 582–594, 2004.
19. **Nomura S, Yamaguchi H, Ogawa M, Wang TC, Lee JR, Goldenring JR.** Alterations in gastric mucosal lineages induced by acute oxyntic atrophy in wild-type and gastrin-deficient mice. *Am J Physiol Gastrointest Liver Physiol* 288: G362–G375, 2005.
20. **Nozaki K, Ogawa M, Williams JA, Lafleur BJ, Ng V, Drapkin RI, Mills JC, Konieczny SF, Nomura S, Goldenring JR.** A molecular signature of gastric metaplasia arising in response to acute parietal cell loss. *Gastroenterology* 134: 511–522, 2008.
21. **Ogawa M, Nomura S, Car BD, Goldenring JR.** Omeprazole treatment ameliorates oxyntic atrophy induced by DMP-777. *Dig Dis Sci* 51: 431–439, 2006.
22. **Ogawa M, Nomura S, Varro A, Wang TC, Goldenring JR.** Altered metaplastic response of waved-2 EGF receptor mutant mice to acute oxyntic atrophy. *Am J Physiol Gastrointest Liver Physiol* 290: G793–G804, 2006.
23. **Parsonnet J, Vandersteen D, Goates J, Sibley RK, Pritikin J, Chang Y.** *Helicobacter pylori* infection in intestinal- and diffuse-type gastric adenocarcinomas. *J Natl Cancer Inst* 83: 640–643, 1991.
25. **Schmidt PH, Lee JR, Joshi V, Playford RJ, Poulsom R, Wright NA, Goldenring JR.** Identification of a metaplastic cell lineage associated with human gastric adenocarcinoma. *Lab Invest* 79: 639–646, 1999.
26. **Stoker M, Gherardi E, Perryman M, Gray J.** Scatter factor is a fibroblast-derived modulator of epithelial cell mobility. *Nature* 327: 239–242, 1987.
27. **Terano A, Hiraishi H, Shimada T, Takahashi M, Yoshiura K, Horie-Sakata K.** Cell culture model for antiulcerogenic agents. *Microsc Res Tech* 53: 389–395, 2001.
28. **Uemura N, Okamoto S, Yamamoto S, Matsumura N, Yamaguchi S, Yamakido M, Taniyama K, Sasaki N, Schlemper RJ.** Helicobacter pylori infection and the development of gastric cancer. *N Engl J Med* 345: 784–789, 2001.
29. **Yamaguchi H, Goldenring JR, Kaminishi M, Lee JR.** Identification of spasmolytic polypeptide expressing metaplasia (SPEM) in remnant gastric cancer and surveillance postgastrectomy biopsies. *Dig Dis Sci* 47: 573–578, 2002.

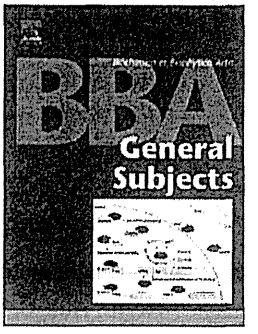

Mitochonrial fumarate reductas as a target of chemotherapy: From patrasites to cancer cells

Chika Sakai, Eriko Tomitsuka, Hiroyasu Esumi, Shigeharu Harada, Kiyoshi Kita

PII: S0304-4165(11)00305-9
DOI: doi: 10.1016/j.bbagen.2011.12.013
Reference: BBAGEN 27149

To appear in: *BBA - General Subjects*

Received date: 27 July 2011
Revised date: 28 November 2011
Accepted date: 17 December 2011

Please cite this article as: Chika Sakai, Eriko Tomitsuka, Hiroyasu Esumi, Shigeharu Harada, Kiyoshi Kita, Mitochonrial fumarate reductas as a target of chemotherapy: From patrasites to cancer cells, *BBA - General Subjects* (2011), doi: 10.1016/j.bbagen.2011.12.013

Mitochonrial fumarate reductas as a target of chemotherapy:

from patrasites to cancer cells

Chika Sakai[a], Eriko Tomitsuka[a, b], Hiroyasu Esumi[b], Shigeharu Harada[c], Kiyoshi Kita[a,1]

[a]*Department of Biomedical Chemistry, Graduate School of Medicine, The University of Tokyo, Tokyo 113-0033, Japan*

[b] *Cancer Physiology Project, Investigative Treatment Division, National Cancer Center Research Institute East, 6-5-1 Kashiwanoha, Kasiwa, Chiba 277-8577, Japan*

[c]*Department of Applied Biology, Graduate School of Science and Technology, Kyoto Institute of Technology, Kyoto 606-8585, Japan*

[1]To whom correspondence should be addressed: Department of Biomedical Chemistry, Graduate School of Medicine, The University of Tokyo, Hongo, Bunkyo-ku, Tokyo 113-0033, Japan. Tel: +81-3-5841-3526; Fax: +81-3-5841-3444; kitak@m.u-tokyo.ac.jp (Kiyoshi Kita)

Kyewords: mitochondrial fumarate respiration, complex II, hypoxia, drug target, *Ascaris suum*, Type II flavoprotein subunit

Abbreviations: FRD, fumarate reductase; L3, 3rd stage larvae; LL3, lung stage L3; MK, menaquinone; SDH, succinate dehydrogenase; SQR, succinate-ubiquinone reductase; TCA cycle, tricarboxylic acid cycle, QFR, quinol-fumarate reductase; RQ, rhodoquinone

Abstract

Recent research on respiratory chain of the parasitic helminth, *Ascaris suum* has shown that the mitochondrial NADH-fumarate reductase system (fumarate respiration), which is composed of complex I (NADH-rhodoquinone reductase), rhodoquinone and complex II (rhodoquinol-fumarate reductase) plays an important role in the anaerobic energy metabolism of adult parasites inhabiting hosts. The enzymes in these parasite-specific pathways are potential target for chemotherapy. We isolated a novel compound, nafuredin, from *Aspergillus niger*, which inhibits NADH-fumarate reductase in helminth mitochondria at nM order. It competes for the quinone-binding site in complex I and shows high selective toxicity to the helminth enzyme. Moreover, nafuredin exerts anthelmintic activity against *Haemonchus contortus* in *in vivo* trials with sheep indicating that mitochondrial complex I is a promising target for chemotherapy. In addition to complex I, complex II is a good target because its catalytic direction is reverse of succinate-ubiquionone reductase in the host complex II. Furthermore, we found atpenin and flutolanil strongly and specifically inhibit mitochondrial complex II.

Interestingly, fumarate respiration was found not only in the prasites but also some types of human cancer cells. Analysis of the mitochondria from the cancer cells identified an anti-helminthic as a specific inhibitor of the fumarate respiration. Role of isoforms of human complex II in the hypoxic condition of cancer cells and fetal tissues is a challenge.

Highlights

Fumarate respiration plays an important role in the anaerobic energy metabolism of parasites.

Fumarate respiration is found not only in the parasites but also some types of human cancer cells.

Fumarate respiration is a good target of chemotherapy for both parasites and cancer.

Important role of human complex II isoforms in the hypoxic condition of cancer cells and fetal tissues

1. Introduction

In the general understanding of bioenergetics of higher eukaryotes, oxygen is a most important terminal electron acceptor of mitochondrial respiratory chain (Fig. 1). The major function of the aerobic respiratory chain is the electrogenic translocation of protons out of the mitochondrial or bacterial membrane to generate the proton motive force that drives ATP synthesis by F_oF_1-ATPase. This mechanism of oxidative phosphorylation is conserved basically from aerobic bacteria to human mitochondria. However, recent study on the respiratory chain of the lower eukaryotes which reside micro-aerophilic environment has shown that the mitochondrial NADH-fumarate reductase system (fumarate respiration) plays an important role in the anaerobic energy metabolism [1]. This system is composed of complex I (NADH-quinone reductase), low potential quinone species and complex II (quinol-fumarate reductase: QFR).

Fumarate respiration is well known electron transport chain in the anaerobic bacteria [2]. Reducing equivalent of NADH is transferred to low potential quinone such as naphthoquione by complex I and finally is oxidized by fumarate by the fumarate reductase activity of complex II which is a reverse reaction of succinate-ubiquinone reductase (SQR) activity of complex II. By using this respiratory chain, bacteria are able to synthesize ATP even in the absence of oxygen. Recent our study of parasitic nematode, *Ascaris suum*, showed fumarate respiration also plays an important role in the anaerobic energy metabolism of adult worms, which reside in the host small intestine where oxygentension is low [1]. Although fumarate reductase activities of bacterial and mitochondrial complex IIs are the same reaction, evolutional positions of each enzyme are quite different. All four subunits of complex II in adult *A. suum* are more closely related to the bacterial and mitochondrial SQR than to bacterial QFR [3-5]. Thus, mitochondrial QFR is a new enzyme evolved by "reverse evolution" of SQR rather than direct evolution from bacterial QFR [6].

Recent our study has revealed that fumarate respiration functions in some human cancer cells and supports a survival of cancer cells in low nutrition and low oxygen conditions [7, 8]. Furthermore, we found complex II with high QFR activity produces reactive oxygen species (ROS) [9]. ROS has been reported to contribute to proliferation and metastasis of cancer cells via the stabilization of hypoxia-inducible factor-1 (HIF-1) [10]. In addition, succinate produced by fumarate respiration also stabilize HIF-1 by the product inhibition of HIF prolyl hydroxylase, which catalyzes the oxygen-dependent hydroxylation of the conserved proline residues in HIF-1 α [11]. Thus, relationship between accumulation of succinate resulted from functional defect of human complex II by the mutation of the subunits and carcinogenesis has recently become a focus of research [8].

As fumarate respiration is essential for the growth and survival of the parasites and some cancer cells, it should be a promising target of chemotherapy for both parasitic diseases and cancer. In this review, we focus on recent advances in the study of parasite and human mitochondrial fumarate respiration and complex II which is an important component of the system [8].

2. Fumarate respiration of parasite mitochondria

2.1 Life Cycle of A. suum and Changes in Respiratory Chain

A. suum is the most widely known parasite, and has been studied as a representative of human and livestock parasites [12-14]. Because of its large size, *A. suum* is an ideal for the study including biochemical analysis. Adult *A. suum* resides in the small intestine of mammals, and the female produces between 200,000 and 400,000 fertilized eggs per day (Fig. 2). Eggs are excreted with feces and become mature eggs containing infectious 3rd stage larvae (L3) in about 2-3 weeks at normal temperature. The eggs reach the small intestine and hatch, when orally ingested by a host. A hatched larva invades the intestinal wall, and migrates to the liver, lung, trachea, and pharyngeal region, and finally returns to the intestine via the esophagus and stomach, and becomes an adult worm. In humans, the larvae of *A. suum* migrate to several organs including liver and lung and cause a wide variety of nonspecific symptoms such as general malaise, cough, liver dysfunction, hypereosinophilia with hepatomegaly and/or pneumonia. The oxygen concentration of the small intestine (~5%) is approximately 25 % of that outside the body, and provides an environment of low oxygen tension in which the energy metabolism of the adult differs considerably from that of the larvae and the host (Fig. 3). The phosphoenolpyruvate carboxykinase (PEPCK)-succinate pathway, an anaerobic glycolytic pathway, operates in the adult worm, producing ATP under such a hypoxic conditions. This system is used by many other parasites such as *Echinococcus multilocularis* [15], and has also been observed in the adductor muscle of oysters and other bivalves that require energy conversion under anaerobic conditions. It is therefore considered to be a very common pathway for energy metabolism in adaptation to hypoxic environment [16, 17].

The first half of the PEPCK-succinate pathway is the same glycolytic pathway found in mammals, in which phosphoenolpyruvate (PEP) is produced. In contrast to aerobic metabolism in mammals involving the conversion of PEP to pyruvate by pyruvate kinase, the *A. suum* adult fixes CO_2 with PEPCK to produce oxaloacetate (OAA). The OAA is converted to malate by the reverse reaction of malate dehydrogenase and transported into the mitochondria to produce pyruvate and fumarate. The NADH formed during production of pyruvate from malate is used in the reduction of fumarate to succinate. The NADH-fumarate reductase system, which is the anaerobic electron transport system characteristic of adult *A. suum* mitochondria, is the final step of this pathway. Unique property of this pathway is discussed in the next section.

In contrast to larvae which require oxygen for their development and possesses the respiratory system to be almost the same as that of mammals, cytochrome *c* oxidase (Complex IV) is not found in the respiratory chain of adult *A. suum* mitochondria, and the content of ubiquinol-cytochrome *c* reductase complex (Complex III) is extremely low [18]. In addition to the enzymes, quinone species in the mitochondria also change during the life cycle of *A. suum*. In contrast to adult mitochondria, in which the low-potential rhodoquinone (RQ ; Em'= -63mV) is the major quinone, ubiquinone (UQ ; Em'= +110mV) is the major quinone of larvae (Fig. 4A) [19]. A combination of SQR and UQ,

and that of QFR and a low-potential quinone, such as RQ or menaquinone (MK), is also observed in *E. coli* and other bacteria during metabolic adaptation to changes in oxygen supply [20, 21]. Lower potential of RQ and MK is favorable for the electron transfer from NADH to fumarate (Fig. 4B). In this way, UQ participates in aerobic metabolism in *A. suum* larva, whereas RQ is participates in anaerobic metabolism in adult *A. suum*.

Although studies have shown a clear difference in energy metabolism between larval and adult *A. suum* mitochondria, little is known about changes in the properties of mitochondria during migration of *A. suum* larvae in the host. As described later, examination of the changes in enzymatic characteristics and subunit composition of *A. suum* larval complex II from lung stage L3 (LL3) larvae obtained from rabbits showed that properties of LL3 mitochondria differed from those of L3 and adult mitochondria [22]. Protein chemical analysis revealed that the change in complex II begins with the anchor subunit, and then occurs in the catalytic subunit. Thus, *A. suum* is able to adapt to changes in oxygen concentration in the environment during its life cycle by dynamic change of respiratory chain.

2.2 NADH-Fumarate reductase system (fumarare respiration) of A. suum adult

The final step of the PEPCK-succinate pathway, which plays such an important role in the anaerobic energy metabolism of the *A. suum* adult, is catalyzed by the NADH-fumarate reductase system as described in the previous section. This system is also called "fumarate respiration". The low-potential rhodoquinone transfers reducing equivalent of NADH via complex I to complex II, and finally succinate is produced by quinol fumarate reductase (QFR) activity of complex II. The merit of this system is to synthesize ATP using the coupling site of complex I even in the absence of oxygen, although its energy efficiency is low (Fig. 5).

A similar anaerobic respiration system exists in the mitochondria of many other parasites, and has also been found in bacteria. Extensive studies of bacteria, including *Escherichia coli*, have revealed the details of this system [23, 24]. In *E. coli*, there are two types of complex II, and QFR encoded by the *frd* operon is induced under anaerobic conditions. A low molecular weight mediator between complex I and complex II is menaquinone (MK; Em'= -80mV), a low-potential naphthoquinone, in the *E. coli* fumarate respiration. In contrast, under aerobic conditions, SQR encoded by *sdh* operon that catalyzes oxidation of succinate is induced [25]. SQR is a dehydrogenase complex in the respiratory system as well as an enzyme in the TCA cycle, and directly connects these systems in aerobic energy metabolism.

Thus, two different enzymes (complex II) are present in *E. coli*, and the bacteria maintain homeostasis of the energy metabolism by controlling synthesis of these enzymes in response to the environmental oxygen supply. How about the complex IIs of *A. suum*? Biochemical and molecular biological analysis showed *A. suum* also possesses two different complex IIs. However, subunit compositions and expression patterns are more complicated in the parasite complex II.